Inspection of Nanofibrous Cloth Defects for Industrial Application

DANIEL HANCIL[1], DARINA JASIKOVA[1] MICHAL KOTEK[1], RADIM KRENEK[2], VACLAV KOPECKY[1]
[1]Institute for Nanomaterials Advanced Technology and Innovation
Technical University of Liberec
Bendlova 1407/7, 461 17 Liberec
CZECH REPUBLIC
[2]Elmarco, s. r. o.
Svarovska, 460 10 Liberec
CZECH REPUBLIC
darina.jasikova@tul.cz http://www.cxi.tul.cz

Abstract: - Performance of electrostatic process, the properties of the fibers and stability of the layer is primarily determined by several limiting conditions such as parameters of process itself, properties of polymer solution, and ambient conditions. Anyway, the conditions of the process are set as ideal the final nanofibers cloth contains defects. Rough defects are seen as droplets of polymer, thinned fibrous layer or impurities that occur from the polymer solution. The local value of defects can not be determined by conventional methods. The analysis of defects of the final product runs in off-line mode without backward loop and progressive intervention to the process, when it exceeds certain amount. The need for a direct link is obvious. Here we present a method of fiber cloth analysis based on line scan camera visualization using various illumination. We detect rough defects using image processing. These defects then evaluate their number determined in the area for each defect and its dimensions in the longitudinal and transverse directions.

Key-Words: - electrospinning, defect detection, visualization, measurement, image analysis, signal processing

1 Introduction

The preparation of nonwoven textiles is one branch of textile industry. Nonwovens of modified nanofibers follow recent trends in filtration, wound heling, affinity membrane, protective clothing, energy generation, enzyme immobilization, drug delivery, scaffolds in tissue engineering, or biomedical applications. [1, 2] Industrial producing of nanofiber cloths is mostly based on electrostatic principles. The methods can be divided into two main categories: needle electrospinning or needless one - electrospinning from free surface (splashing electrospinning, rotating drum - solid cylindrical electrode, rotating spiral wire electrode, disc collector, and sharp pin inside the rotating collector, knife-edged electrodes, and single wire electrode). [3-5]

Last mentioned method, electrospinning from single wire electrode, is world well known as the Nanospider™ technology [6]. This technique raised under evolution of rotating drum technique in order to decrease user contact with solvents and to increase the effect of the process. This process is based on stationary, charged single wire electrode. The solution is applied to the electrode using an applicator head, so called carriage with reservoir. The fibers are collected on substrate between the spinning and the opposite grounded plate electrode. As spinning wire electrode (SE) is covered with a polymeric solution, it is immediately divided into separate droplet and spinning jets start from them. The behavior of the jet depends on the properties of polymer solution (viscosity, conductivity, surface tension) as well as the applied voltage and surrounding effecting character of electric field. [7, 8]

The basic parameter is the presence of polymer solution on the wire. Thickness of coating polymer layer is influencing process yield, fiber diameter, distribution of Taylor jets. This parameter can be regulated with movement velocity of applicator head.

Anyway, the conditions of the process are set as ideal the final nanofibres cloth contains defects. Rough defects are seen as droplets of polymer, thinned fibrous layer or impurities that occur from the polymer solution. The nanofiber material undergoing final inspection before it reaches the

customer. So far, this control was based on random inspection. There were taken samples further analyzed in laboratory. This inspection contains scanning, defect analysis, fiber valuation on diameter and surface quality. The industrial are capable of producing tens of millions of square meters of material per year of nanofibrous cloth.

Following high quality outcome, these controls have to be fulfilled with continuous monitoring system. This system should reveal the rough defects just after the production, and should be part of the machine. Here we present the procedure of development of the monitoring system that consists of hardware part for illuminating and capturing fibrous layer as well as further analysis.

2 Materials and Methods

The analysis of defects of nanofibrous layer is examined in off-line mode. The basic method is scanning of random selected samples. There is tested 196 cm^2 of material on one roll of fabricated material. These samples are tested on defects in a given area (density) and a water column acting on membrane sample. It is the one of key parameters of membranes. The selected samples are monitored in five places evenly distributed over the whole width of the roll.

2.1 Water Column Testing Method

The study revealed a significant deviation of these two parameters. There is high number of defects on one side of roll. This correspond low value of the water column. Shapes and distribution of parameters not correlate. Both parameters oscillate longitudinally due to destructive nature of measurement methods. Therefor it is impossible test one sample twice. There were used samples of material taken very close to each other.

a)

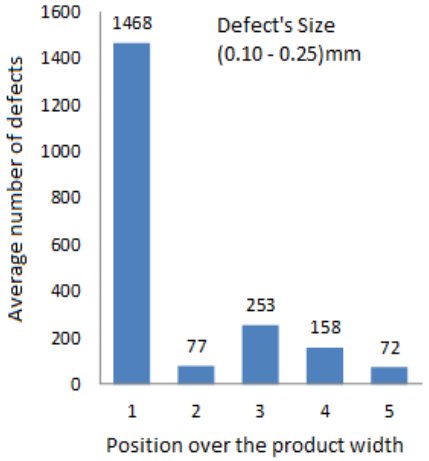

b)

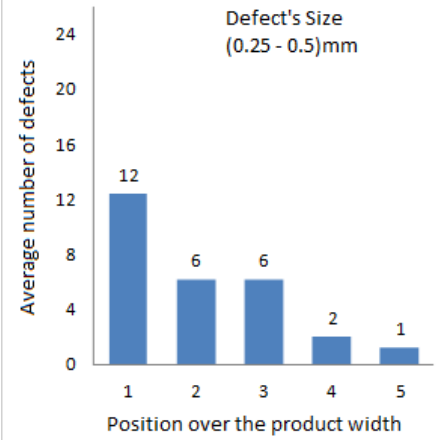

c)

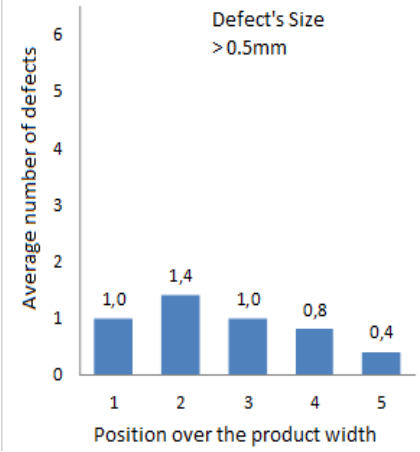

Fig. 1 Statistics of defects diameter is dependent on the position of sample in axial axis of roll. Defects population grows roughly exponentially with decreasing size of the defect. Significant increase in incidence is observed in the 1st position (region for machine control).

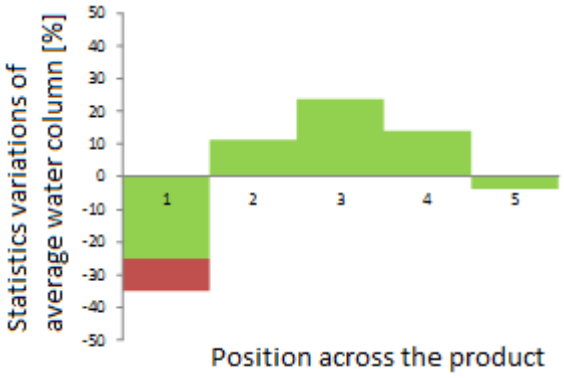

Fig. 2 Statistics variations of the water column (target product parameter) measurement are relative to the defect diameter.

Statistics variation is depending on the sampling position in the transverse direction of the membrane roll. Significantly reducing the water column in the 1st position, the others are statistically insignificant due to the normal variation coefficient of 25% error of the measurement method on membranes (ISO 811).

Result convinces us to correlate defect density and the water column. Off-line method for the measurement defects and the water column are very time consuming methods, hence the need for the industry to introduce online mode directly on the production line. This is particularly useful for scanning of defects.

2.1 Identification System

The identification system is based on CCD camera, lens system and lightening unit. The requirements of industrial system take in account parameters such as depth of field, pixel sensitivity, speed of transfer, resolution and space requirements. Here we have chosen line scan camera Basler raL8192-12gm. This camera is equipped with Awaiba DR-8k-3.5 CMOS chip with resolution 8192 px and single pixel size of (3.5x3.5) um. The maximal sampling frequency is 12 kHz. The GigE connection technology enables high speed data transfer.

Scanning area was set at 70 mm width. Single pixel corresponds to 8.5 um accuracy using distance calibration and with 8192 pixel resolution. This setup covers the need of detection defects of size above 100 um very well.

The camera was fitted with lens system Componon-S 4.0/80-0022. Unlike conventional camera lenses where the optical performance decreases as the magnification increases, Schneider-Kreuznach macro lenses have been developed and corrected for the close-up range of 1:20 to 1:1. Due to its mechanical stability and the robust V-mount interface enabling simpler adjustment of the azimuth position. Here we used the set of extensions to reach the magnification and increase the focusing distance. The focusing distance can be calculated following relation (1).

$$a_n = \frac{f^2}{d_m + \frac{f^2}{a-f}} + f \qquad (1)$$

, where a is focusing distance of the lens system, f focal a d_m is the width of extensions.

This condition enables change unlimited focusing distance to maximal, for example 400mm using lens system with focal 80mm and with of extensions 20mm.

The continuous LED light source Edmund Optics was used as a linear lightening unit. The light source was fitted with diffuse cover. The lighting unit was fixed on rotary arm. This enables varying work distance and angles towards optical axis of camera in the range between 10°and 90°. This setup enables changes of lighting principles i.e. bright and dark field.

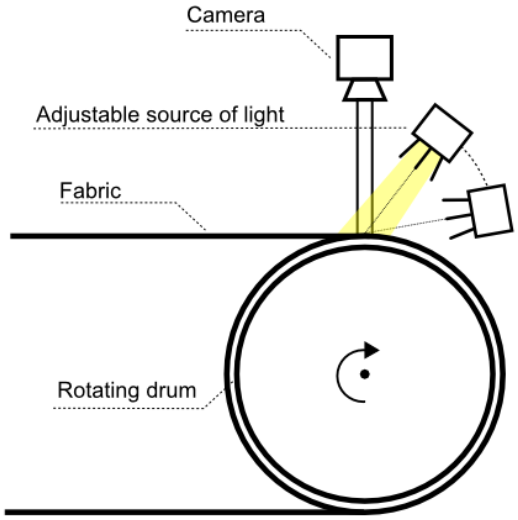

Fig. 3 Schema of the visualization system.

The nanofibres cloth is withdraw from the spinning chamber using rotary drum and further collected on the roll. The rotary drum is fitted with the lightening system and camera unit as it is seen in Fig. 3. The nanofiber layer is deposited on the matrix nonwoven material. Due the matrix structure it is impossible use screening technique for defects detection. The movement of fabrics is controlled by the drum rotation. The axis of rotation is intuitively in axis of drum. We place the camera and lightening unit according to the drum rotation and application of the line scan camera is optimal due the limited focusing depth. The testing drum's diameter was 290 mm and angular velocity approximately 0.18 rad / sec.

Angular velocity can be defined as:

$$\omega = \frac{d\varphi}{dt}$$, or as vector $$\boldsymbol{\omega} = \frac{\boldsymbol{r} \times \boldsymbol{v}}{|\boldsymbol{r}^2|} \qquad (2)$$

, where vector ω is perpendicular to the to the plane formed by the position vector r and velocity vector v, rotation axis direction (thrust vector) and vectors ω, r, v thus forming a right-handed system.

We can determine the speed and the peripheral is about 26.1 mm/s using this analysis. The exposure time is dependent on the velocity and light intensity. It was set 3.2 ms in this case, as the base line rate is 3054 per second. The final line rate was 2950 rps following distance the calibration. Using this calibration on the camera resolution, we obtain space resolution of (8192 x 3544) px with the frame rate of 0, 83 images per second. The system is seen in Fig. 3.

The lightening system was set according to the basic postulate of optical physics. The refracted angle of light from the object corresponds with the angle of illumination ϕ_r.

$$\phi_r = \phi_i \tag{3}$$

The difference between Dark and Bright field approach is in the angle between the lighting and the camera. Bright field principle is suitable for contrast but consuming specular reflection from lighting into the camera. It is very difficult to avoid Hot spots.

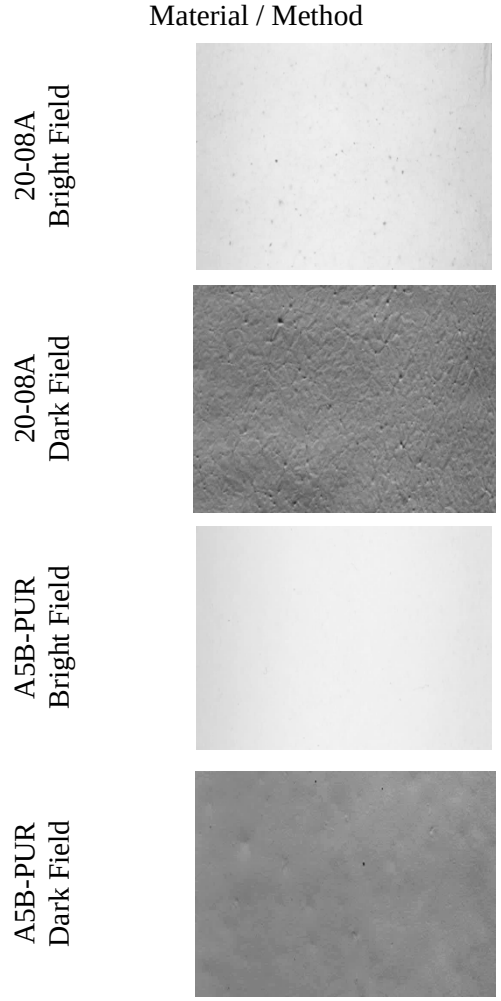

Fig. 4 Pictures in the first row shows the difference in illumination for material of inner marking 20-08A, the second row is for the material A5B-PUR

Oppositely, the Dark Field approach is logically defined with the range of angles from 45 ° to 90 °. The light in this case is reflected away from the lens system. The light diffuse and the reflected light creates the pattern. This lightening principle is suitable for textures, material surface structures and height distinct objects. It is used for capturing and scanning of laser engraved or burned marks. This method increased the contrast of thin objects on the shiny background. It is obvious that type of lighting excel others details. The Bright field enables contrast; on the other hand the Dark Filed provides information of reliefs [9].

3 Image Processing of Detect

The automatically diagnosis of defects is based on the hardware solution as well as the data processing sequence. The data analyzing apparatus starts at line camera with image processing, resp. reconstruction of line resolution into the 2D camera resolution creating and following x and y axis of pixels.

Images for automatic evaluation has to be pre-processed using brightness balance, blurring, edge detection, threshold function, noise reduction. It is important to note that these adjustments bring no new information in terms of entropy [10]. Each additional operations decrease complex predictive value at the expense of single characteristics. Redundancy of information often uses the picture for human purposes. The great example could be brightness correction.

Common view on the captured image requires no changes of brightness along the x axis. However, the situation changed after the histogram equalization according to (4)

$$I' = \frac{1}{XY}\sum_{i=I_0}^{i=I} H(i) \tag{4}$$

, where I is the initial intensity, X a Y are picture diameters, I_0 is the lowest intensity of initial image and $H(i)$ is the component of histogram.

This modified image is then seen in figure 5. The brightness correction brought out the calibration need. The shadow on the edges is induced by extensions between the lens system and the camera chip. The brightness shift makes impossible further

image processing due low contrast of information, i.e. surface defects on the background of fiber layer.

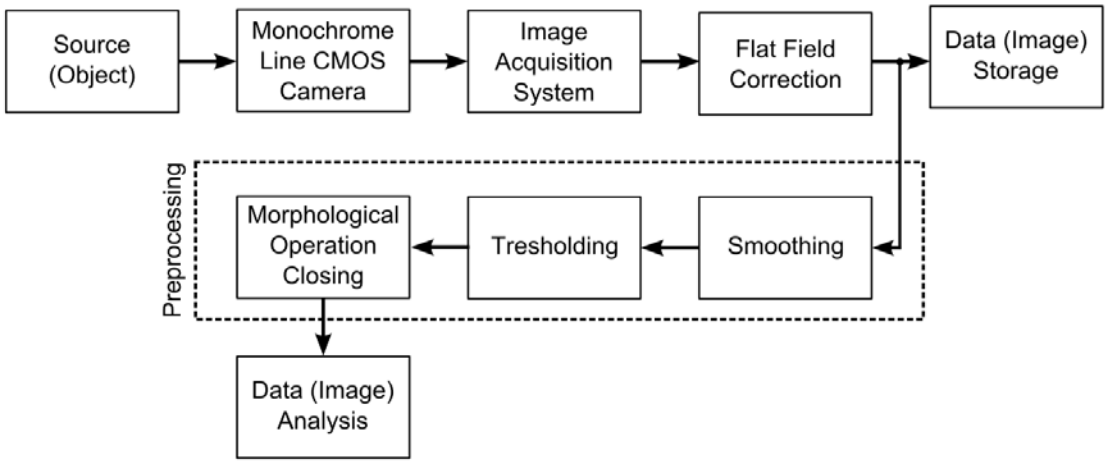

Fig. 5 Schema of image pre-processing and processing algorithm with data analysis sequence.

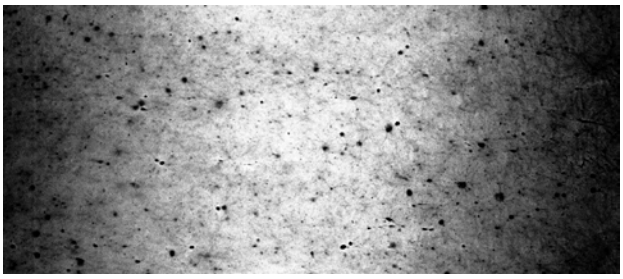

Fig. 6 Row camera view.

Series of images with uniform underground was captured to calibration. There were also determined levels in which the Line profiles (profile of intensities according to line) were extracted. These line profiles are averaged by the set of images and result is shown in the graph ... There is even shown the quadratic function interpolation with parameters $a_0 = -2E^{-06}$, $a_1 = 0.0164$ and $a_2 = 152.11$, which can provide a corrected picture.

$$y = -2.10^{-6}x^2 + 0{,}0164x + 152{,}11 \quad (5)$$

Differences between original and corrected image (material 20-08A, both after the histogram equalization – formula (4)) can be seen in figure (5) and (6).

As mentioned above, smoothing is one of the first and basic procedures of image preprocessing. It is important both for human observation and for using a segmentation algorithm thresholding – smoothing reduces unpleasant impact of noise. In this case, filtration by the Gaussian kernel was used following relation (7).

$$G(x,y) = \frac{1}{2\pi\sigma^2} e^{\frac{x^2+y^2}{2\sigma^2}} \quad (7)$$

, where x and y are distances from origin and σ is the standard deviation.

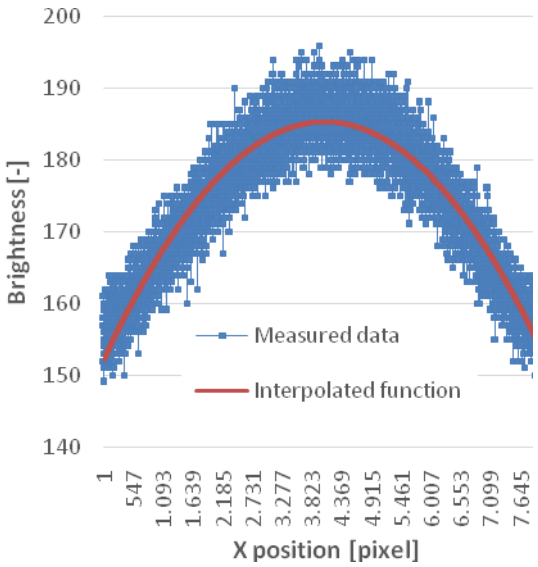

Fig. 7 Interpolated function of the raw camera view for the further data pre-processing brightness calibration and compensation.

The segmentation was followed by thresholding (detected objects are characterized lower brightness compared to surrounding). After this procedure of binarization it is necessary to remove small particles caused mainly by noise and close object boundaries [11]. For this purpose the function „Close“ coming from the group of operations called “Binary morphology”. Morphological closing algorithm, which consists of morphological dilatation followed by erosion according to equation, is applied to simplify the edges of detected dark area.

$$X \cdot B = (X \oplus B) \ominus B \quad (8)$$

, where X is the image and B the structure element and

$$X \oplus B = \{p \epsilon \varepsilon^2 : p = x + b, x \epsilon X \text{ and } b \epsilon B\}$$

, and

$$X \ominus B = \{p \epsilon \varepsilon^2 : p + b \epsilon X \text{ for every } b \epsilon B\}$$

Due to knowledge of the scene and expected shapes of contour it was used the round structure element with dimensions 7x7.

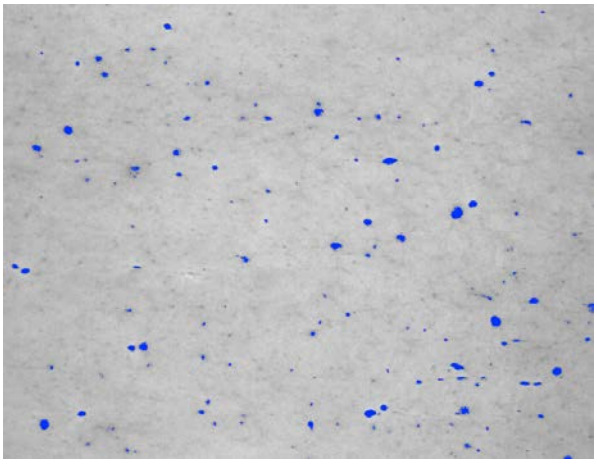

Fig. 8 Resulting image with blue marked identified defects.

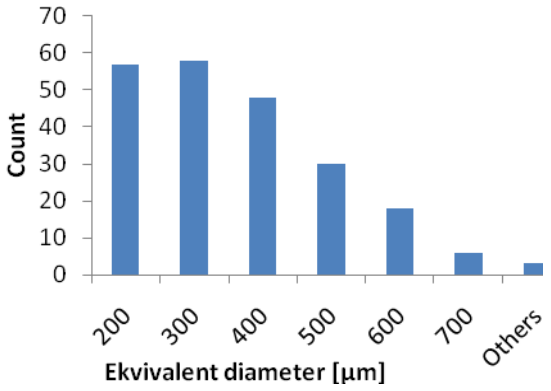

Fig. 9 Histogram of defects according to their diameter over selected sample.

4 Conclusion

The image obtained from the line camera was subsequently analyzed. There was designed and implemented own software for finding and identifying defects in the image and their evaluation. The algorithm uses the reconstructed image containing morphological mathematical operations, thresholding and other methods of image analysis reveals defects. These defects then evaluate their number determined in the area for each defect and its dimensions in the longitudinal and transverse directions. This progress in fibrous layer analysis on the outlet of the process significantly contributes to increase of filter quality and safe energy and time of product evaluation.

The authors gratefully thank to the support of Technology Agency of the Czech Republic (TA ČR) TA04011086 - Opto-electronic system for quality control of nanofiber materials production, and LO1201 co-funding from the Ministry of Education, Youth and Sports as part of targeted support from the „National Programme for Sustainability I".

References:

[1] D. H. Reneker, A. L. Yarin, Electrospinning jets and polymer nanofibers, *Polymer* 49, 2008, pp. 2387-2425.

[2] N. Bhardwaj, S. C. Kundu, Electrospinning: A fascinating fiber fabrication technique, *Biotechnology Advances* 28, 2010, pp. 325-347.

[3] D. Nurwaha, X. Wang, Free Surface Electrospinning: Investigation of the Combined Effects of Process Parameters on the Morphology of Electrospun Fibers, *Fibers and Polymers* 16, 4, 2015, pp. 850-866.

[4] K. M. Forward, A. Flores, G. C. Rutledge, Production of core/shell fibers by electrospinning from a free surface, *Chemical Engineering Science* 104, 2013, pp. 250-259.

[5] K. M. Forward, G. C. Rutledge, Free surface electrospinning from a wire electrode, *Chemical Engineering Science* 183, 2012, pp. 492-503.

[6] Elmarco s.r.o., Method for application of liquid polymeric material onto spinning cords and a device for production of nanofibers through electrostatic spinning, WO/2012/139533, 10.18.2012.

[7] X. Yan, M. Gelvelber, Investigation of Electrospun fiber diameter distribution and process variations, *J. of Electrostatics* 68, 2010, pp. 458-464.

[8] Y. Cai, M. Gelvelber, The effect of relative humidity and evaporation rate on electrospinning: fiber diameter and measurement for control implications, *J Mater Sci*, 2013, pp. 1-15.

[9] A. Ryer, *Light measurement handbook*, 1997.

[10] R. M. Haralick, L. G. Shapiro, *Computer and Robot Vision*, Addison-Wesley Longman Publishing Co., Inc., Boston, MA, USA, 1992.

[11] J. Serra, *Image Analysis and Mathematical Morphology*. Academic Press, Inc., Orlando, FL, USA, 1983.